Type of contribution:
Editorial
▶ Research Paper
Case Study
Review Paper
Scientific Data
Report of Tech. Application

mesi
e-issn. 2798-5245

Mechanical Engineering for Society and Industry
Vol. 6, No. 1 (2026) pp 114-127
https://doi.org/10.31603/mesi.15295

Corrosion behavior of ST37 low carbon steel welded joints in acidic and basic environments: Implications for structural durability

Andika Wisnujati[1]*, Mudjijana[2], Syamsul Ma'arif[3], Satriardi[4], Hojjat Bagban[5]

[1] Department of Automotive Engineering Technology, Universitas Muhammadiyah Yogyakarta, Bantul 55184, **Indonesia**
[2] Department of Mechanical Engineering, Universitas Muhammadiyah Yogyakarta, Bantul 55184, **Indonesia**
[3] Department of Industrial Engineering, Universitas Sarjanawiyata Tamansiswa, Yogyakarta 55165, **Indonesia**
[4] Department of Industrial Engineering, Universitas Muhammadiyah Riau, Pekanbaru 28156, **Indonesia**
[5] Department of Artificial Intelligence, Chang Gung University, Taoyuan 333, **Taiwan**
✉ andikawisnujati@umy.ac.id

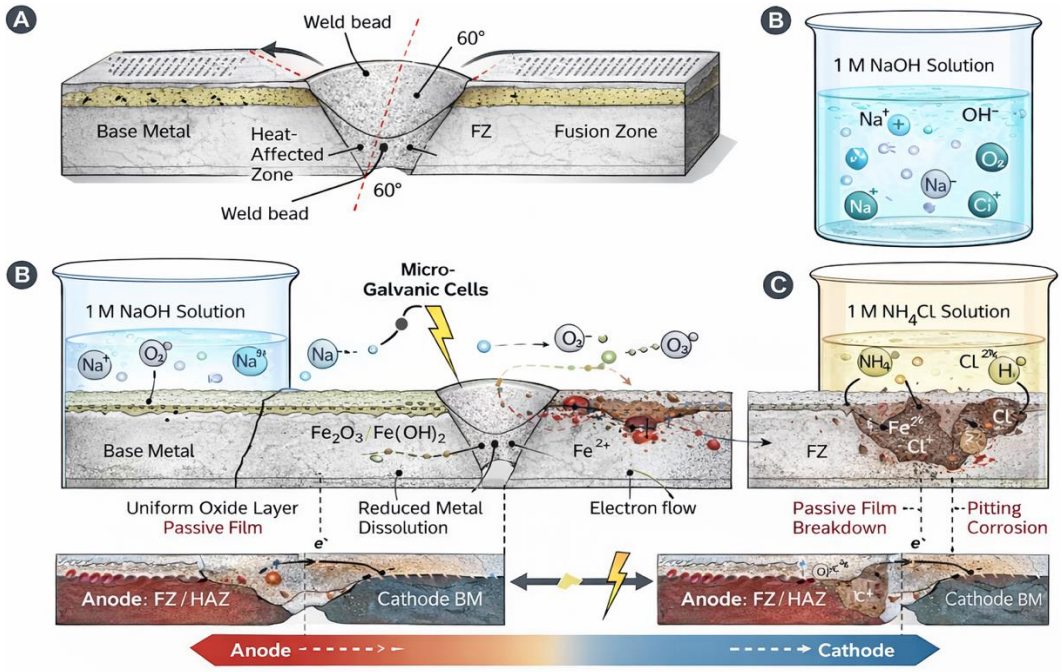

Article info
Submitted: 2025-11-11
Revised: 2026-03-10
Accepted: 2026-03-30

Publisher
Universitas Muhammadiyah Magelang

Highlights:

- Welded ST37 low-carbon steel was evaluated for corrosion and mechanical degradation in 1 M NaOH and 1 M NH_4Cl environments at different immersion times.
- NaOH exposure promoted the formation of a stable oxide layer, resulting in lower corrosion rates and partial recovery of tensile strength after prolonged immersion.
- NH_4Cl exposure caused more severe localized corrosion, including pitting, porous corrosion products, and passive film breakdown due to chloride attack.
- SEM–EDS analysis confirmed solution-dependent corrosion mechanisms, with thicker corrosion layers in the weld region and increased oxygen and chloride contents after immersion.
- The findings highlight the critical role of solution chemistry and exposure duration in determining the durability of welded ST37 steel structures.

Abstract

This study investigates the corrosion behavior and mechanical degradation of welded ST37 low-carbon steel exposed to basic (NaOH) and chloride-containing (NH_4Cl) environments. The objective is to evaluate the influence of solution chemistry and immersion time on corrosion rate, surface

morphology, elemental composition, and tensile properties of welded steel structures. Welded ST37 specimens were immersed in 1 M NaOH and 1 M NH_4Cl solutions for 100, 200, and 300 hours under controlled laboratory conditions. Corrosion rates were determined using the weight loss method, while surface morphology and elemental composition were analyzed using scanning electron microscopy coupled with energy dispersive spectroscopy (SEM–EDS). Mechanical degradation was evaluated through tensile testing following ASTM E8 standards. The results show that NaOH exposure promotes the formation of a stable oxide layer that reduces corrosion rates from 0.024 to 0.019 mm/year and partially restores tensile strength after prolonged immersion. In contrast, NH_4Cl exposure causes more aggressive corrosion characterized by pitting, porous corrosion products, and localized surface degradation due to chloride-induced passive film breakdown. SEM observations confirm thicker corrosion layers and localized attack in the weld metal region, while EDS analysis reveals increased oxygen and chloride content associated with the respective corrosion mechanisms.

Keywords: ST37 low-carbon steel; Corrosion behaviour; NH4Cl and NaOH environments; SEM-EDS analysis

1. Introduction

Corrosion remains one of the most critical degradation phenomena limiting the structural integrity, service reliability, and operational safety of metallic components in industrial systems [1], [2]. Low-carbon steels are particularly vulnerable due to their thermodynamic instability in aggressive chemical environments, despite their widespread adoption owing to favorable mechanical properties, weldability, and cost efficiency. Among these materials, ST37 low-carbon steel is extensively utilized in structural frameworks, pipelines, automotive components, and manufacturing equipment because of its high ductility, formability, and economic availability [3]. However, the long-term durability of ST37 low-carbon steel is strongly influenced by environmental exposure conditions. In acidic and basic media commonly encountered in chemical processing plants, wastewater systems, marine atmospheres, and industrial cleaning operations electrochemical reactions at the metal environment interface can significantly accelerate material degradation. The interaction between solution chemistry, surface film stability, and microstructural heterogeneity plays a decisive role in governing corrosion kinetics and damage evolution. Consequently, understanding the corrosion behavior of ST37 low-carbon steel under controlled pH conditions is essential for predicting service life and optimizing protective strategies in industrial applications [4], [5].

Welding is a fundamental joining process in metal fabrication and is widely applied in structural and industrial manufacturing sectors [6], [7]. Notwithstanding its significance, the welding process induces localized discrepancies in microstructure, residual stress, and phase composition, potentially making welded areas more vulnerable to corrosion than the underlying metal. Metallurgical and mechanical modifications might undermine the electrochemical stability of the weldment, facilitating localized corrosion phenomena such as pitting, crevice corrosion, and intergranular attack [8], [9]. A thorough comprehension of the corrosion characteristics of welded joints is essential for ensuring the long-term durability and structural integrity of components made from ST37 low-carbon steel [10].

The study of corrosion mechanisms in welded joints requires simulation of actual service environments, which often involve contact with acidic or basic chemical substances. Acidic environments are typically rich in chloride ions (Cl^-), such as those present in ammonium chloride (NH_4Cl) solutions, which accelerate the corrosion process through anodic dissolution and pitting corrosion. Basic environments, on the other hand, may arise from the presence of sodium hydroxide (NaOH) in processes such as chemical cleaning, industrial wastewater, or alkaline battery systems. Although NaOH solutions are generally less aggressive than acidic media, they can still induce significant corrosion under certain conditions, particularly through stress corrosion cracking and passive layer destabilization [11], [12].

In welded joints, three principal zones can be distinguished base metal, fusion zone, and heat-affected zone each exhibiting unique microstructural features that govern their corrosion behavior. The base metal retains its original ferrite–pearlite structure and generally shows uniform corrosion resistance. The fusion zone, formed by solidification of the molten weld pool, often contains columnar grains and segregated alloying elements, which can promote localized corrosion due to compositional heterogeneity. The heat-affected zone, subjected to thermal cycling without melting, undergoes grain coarsening and phase transformations that typically reduce its corrosion

resistance, making it the most vulnerable region to pitting or intergranular attack. Transitional interfaces between these zones further intensify galvanic interactions, accelerating localized degradation. Thus, the heterogeneous nature of welded joints necessitates zone-specific analysis, as emphasized by Huang *et al*. [13], to fully understand the mechanisms of corrosion and the reliability of welded structures in aggressive environments. However, limited research has focused specifically on the comparative behavior of ST37 low-carbon steel welded joints in both acidic and basic solutions under controlled laboratory conditions. Understanding this comparative behavior is crucial, particularly for engineering applications where such materials are exposed to fluctuating pH conditions due to operational requirements or environmental exposure [14], [15], [16].

Influence of Partial Rust Layer on the Passivation and Chloride-Induced Corrosion of Q235b Steel in the Carbonated Simulated Concrete Pore Solution Li *et al*. [17] examined how pre-existing rust layers affect passivation and subsequent chloride attack in low-carbon steel. Their findings highlight how localized damage in welded zones may compromise corrosion resistance an insight relevant to the welded ST37 low-carbon steel specimens in this study. Palanivelu *et al*. [18] compared corrosion rates of different manufacturing grades of mild steel under acidic and basic environments. The results underscore how microstructural heterogeneities (such as those in welded zones) influence corrosion behavior. Case Study from Tyrala and Pawlowski [19] provided a detailed SEM/EDS investigation of pit initiation and growth in welded steel pipes, attributing accelerated failure to weld zone metallurgical changes and chloride exposure.

The corrosion mechanisms in a welded joint of ST37 low-carbon steel under acidic and basic environments through four schematic sections (A–D) that illustrates in **Figure 1**. In (A), the cross-sectional configuration of the welded joint is presented, highlighting the base metal (BM), heat-affected zone (HAZ), and fusion zone (FZ) [20]. The welding thermal cycle produces microstructural and compositional heterogeneity across these regions, leading to electrochemical potential differences that may initiate localized corrosion when exposed to an electrolyte. In (B), the corrosion mechanism in 1 M NaOH solution is depicted, where hydroxide ions promote the formation of a stable passive film composed mainly of iron oxides and hydroxides. This uniform oxide layer acts as a protective barrier, reducing anodic dissolution and resulting in relatively low and uniform corrosion rates [21].

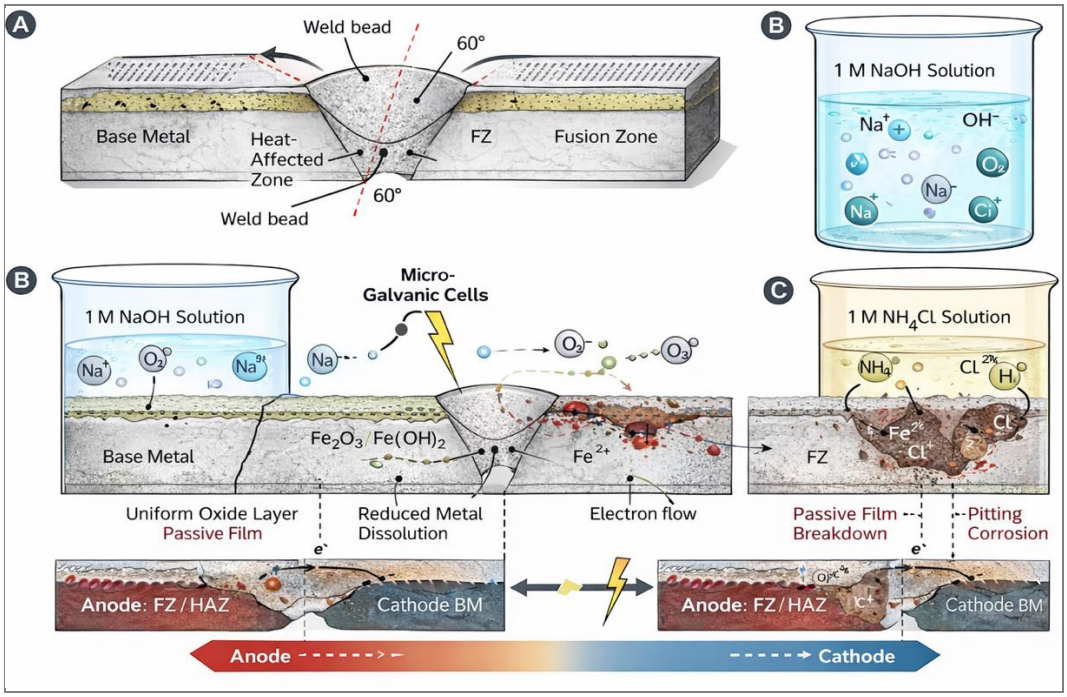

Figure 1. Schematic illustration of corrosion mechanisms in welded ST37 low-carbon steel joint under acidic and basic environments

In contrast, (C) represents the behavior in 1 M NH_4Cl solution, where chloride ions penetrate and destabilize the passive film, leading to localized passive film breakdown and pitting corrosion, particularly in the FZ and HAZ regions. The formation of soluble iron chloride species accelerates metal dissolution and intensifies localized attack. Finally, (D) schematically shows the micro-galvanic coupling mechanism within the welded joint, where the FZ or HAZ may function as anodic regions and the BM as the cathodic region. Electron flow between these regions enhances localized corrosion, especially in chloride-containing environments. Together, sections (A–D) emphasize the

combined influence of weld-induced microstructural heterogeneity and solution chemistry on the corrosion behavior of ST37 low-carbon steel welded joints.

A localized dissolution and pit nucleation are the results of chloride-containing environments, which promote passive film disintegration through competitive adsorption of Cl^- ions from an electrochemical perspective [22]. Conversely, the formation of protective iron oxides or hydroxides may be induced by basic environments, which could potentially reduce corrosion kinetics through passivation mechanisms. Nevertheless, these anticipated behaviors may be modified by the presence of microstructural gradients induced by welding.

Therefore, this study aims to:

- Quantitatively compare corrosion kinetics of welded ST37 low-carbon steel in 1 M NH_4Cl and 1 M NaOH solutions.
- Characterize surface degradation mechanisms using SEM–EDS analysis.
- Evaluate the correlation between corrosion progression and tensile strength degradation.
- Clarify whether welded zones act as preferential corrosion initiation sites under different pH conditions.

By integrating gravimetric analysis, microstructural observation, and mechanical testing, this study provides a mechanistic understanding of corrosion–strength interaction in welded low-carbon steel structures. The findings contribute to predictive maintenance strategies, welding parameter optimization, and corrosion mitigation design in industrial applications where steel structures operate under variable chemical exposures.

2. Methods and Material

2.1. Research Methodology Framework

This study employed a systematic experimental framework to investigate the corrosion behavior and mechanical degradation of welded ST37 low-carbon steel in acidic and basic environments. The overall research workflow is illustrated in **Figure 2**, which outlines the sequential stages of the study from problem identification to data interpretation.

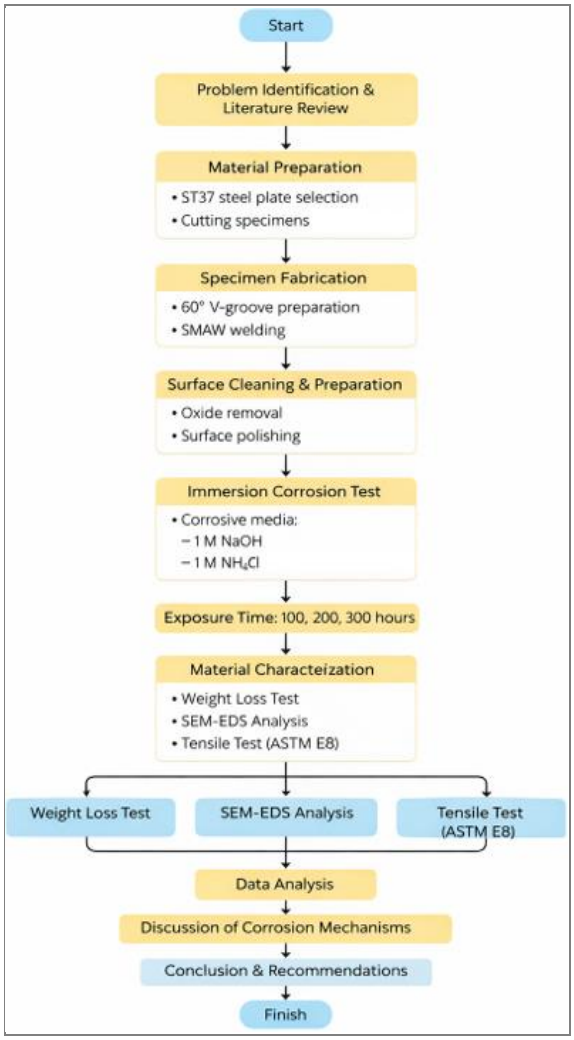

Figure 2. The experimental framework for assessing the corrosion characteristics of welded ST37 low-carbon steel

The research began with problem identification and literature review to understand corrosion mechanisms affecting welded low-carbon steel exposed to aggressive chemical environments. Previous studies on corrosion kinetics, weld joint degradation, and electrochemical interactions in acidic and basic media were analyzed to establish the research objectives and experimental design. Following this stage, material preparation was conducted using ST37 low-carbon steel plates. The plates were cut into specimens with predetermined dimensions to ensure uniformity across all samples. The specimens were then subjected to specimen fabrication, which included the preparation of a 60° V-groove joint followed by the Shielded Metal Arc Welding (SMAW) process. The welding procedure was performed under controlled conditions to ensure consistent weld penetration and joint quality [3].

After welding, the specimens underwent surface cleaning and preparation to remove oxide layers, welding residues, and surface

contaminants that could influence corrosion behavior. Surface polishing and cleaning procedures were conducted to achieve uniform surface conditions prior to corrosion testing [23]. The prepared specimens were subsequently subjected to immersion corrosion testing in two corrosive environments: 1 M sodium hydroxide (NaOH) representing an basic medium and 1 M ammonium chloride (NH_4Cl) representing a chloride-containing environment. Each specimen was immersed for 100, 200, and 300 hours under controlled laboratory conditions.

2.2. Material Specification

The material preparation involved cutting ST37 low-carbon steel, followed by welding and surface cleaning of the specimens. Subsequently, the samples were immersed in corrosive solutions of acid (NH_4Cl) and base (NaOH) for exposure periods of 100, 200, and 300 hours. **Figure 3** depicts the preparation procedure of ST37 low-carbon steel specimens with an initial thickness of 10 mm. The plates were first sectioned into dimensions of 3 × 15 mm, yielding six specimens. A 60° V-groove was subsequently machined along the joint interface to facilitate proper weld penetration. The specimens were then joined using a welding process, producing welded samples with overall cross-sectional dimensions of 30 × 30 mm. This preparation procedure ensured dimensional consistency and geometric uniformity of the welded joints prior to mechanical and corrosion testing.

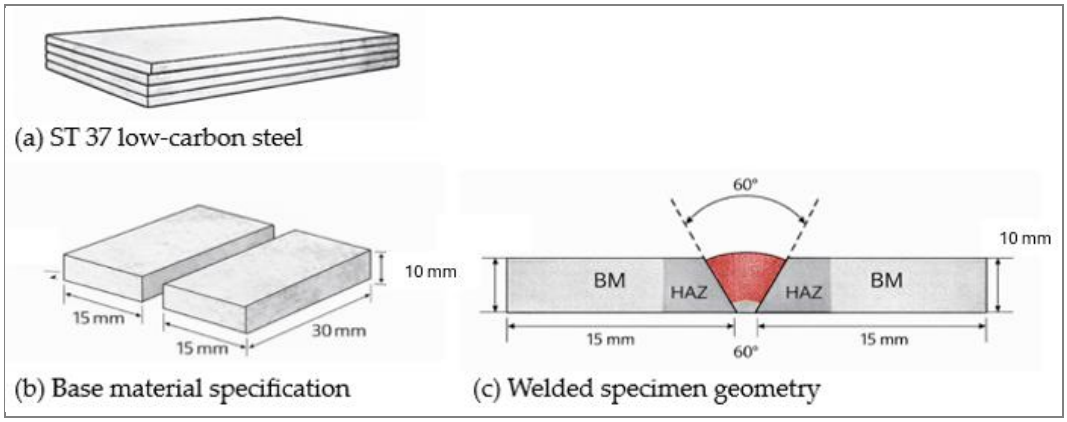

Figure 3. Specimen fabrication procedure of ST 37 low-carbon steel: (a) Base material specification (10 mm thickness); (b) Geometry of ST37 low-carbon steel coupons (30 × 15 × 10 mm) prepared for V-groove butt welding, and (c) Cross-section of 60° V-groove welded ST37 low-carbon steel joint

2.3. Physical and Mechanical Properties

The corrosion resistance testing phase incorporated three complementary analyses [24], [25]. The weight loss test was performed to determine the corrosion rate based on the reduction in specimen mass. **Figure 4** illustrates the corrosion mechanism of ST37 low carbon steel exposed to an aqueous electrolyte containing dissolved oxygen and chloride ions. The corrosion process initiates at anodic regions on the steel surface, where iron undergoes oxidation according to the reaction $Fe \rightarrow Fe^{2+} + 2e^-$. The released electrons migrate to adjacent cathodic areas, where oxygen reduction occurs in the presence of water, forming hydroxide ions ($O_2 + 2H_2O + 4e^- \rightarrow 4OH^-$).

The generated Fe^{2+} ions subsequently react with OH^- ions to form iron hydroxides, which further oxidize into hydrated iron oxides (rust). The presence of chloride ions (Cl^-) destabilizes the passive layer and promotes localized attack, leading to pitting corrosion. Additionally, restricted oxygen diffusion within confined geometries results in differential aeration cells, accelerating crevice corrosion. These localized electrochemical processes collectively contribute to material degradation and thickness reduction in ST37 low carbon steel under corrosive environments.

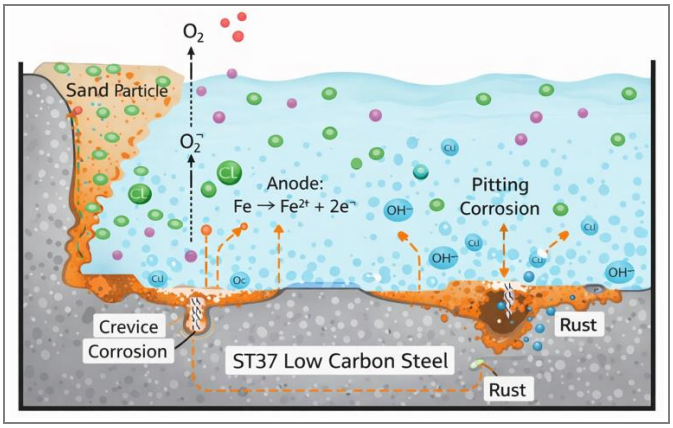

Figure 4. Illustrates the corrosion mechanism of ST37 low carbon steel

In addition, Scanning Electron Microscopy coupled with Energy Dispersive Spectroscopy (SEM-EDS) was employed to examine surface morphology and to identify elemental changes on the steel surface after immersion [26]. The corrosion rate was determined using the weight loss method, based on the mass loss

(ΔW) of the specimen over a known surface area (A) and exposure time (t), with constant (C) and material density (ρ).

The tensile properties of ST37 low-carbon steel in Figure 5 were evaluated in accordance with ASTM E8 standard test methods for tension testing of metallic materials. Rectangular specimens were machined from the base plate and welded joint region using precision cutting to ensure dimensional accuracy and uniform geometry. The specimen dimensions were prepared according to subsize specimen requirements specified in ASTM E8, considering the 1 mm plate thickness. The gauge length and width were carefully controlled to minimize geometric variability and ensure repeatability of results.

The methodological framework employed in this study follows established corrosion testing standards, with strictly controlled parameters including solution composition, electrolyte volume-to-specimen ratio, and exposure duration. NH_4Cl was selected due to its practical relevance in industrial cooling systems, whereas NaOH represents a commonly encountered basic medium in various industrial operations. Deionized water was utilized to minimize interference from extraneous ionic species, thereby ensuring more accurate interpretation of corrosion behavior [27].

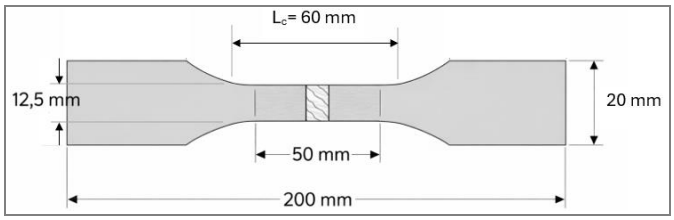

Figure 5. Tensile test specimen of ST37 low-carbon steel to standard dimensions in accordance with ASTM E8

3. Results and Discussion

3.1. Surface Morphology and Corrosion Behavior

The surface morphology of ST37 low-carbon steel after immersion revealed distinct corrosion characteristics between the NaOH and NH_4Cl solutions. SEM observation showed that samples exposed to NaOH developed a relatively uniform oxide layer, indicating the formation of a stable passive film that limited further metal dissolution. In contrast, specimens immersed in NH_4Cl exhibited rough and porous surfaces with evidence of pitting corrosion caused by chloride ion attack. The surface morphology of ST37 low-carbon steel after immersion in NaOH and NH_4Cl solutions for 100, 200, and 300 hours, as shown in Figure 6 to Figure 9, reveals distinct corrosion behaviors associated with the chemical environments.

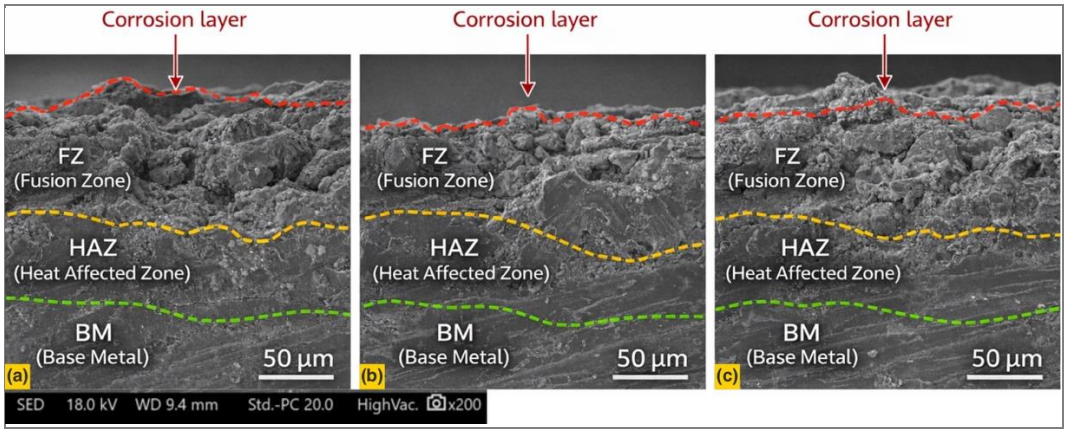

Figure 6. Cross section material ST37 low-carbon steel after immersion NaOH: (a) 100 hours; (b) 200 hours; (c) 300 hours

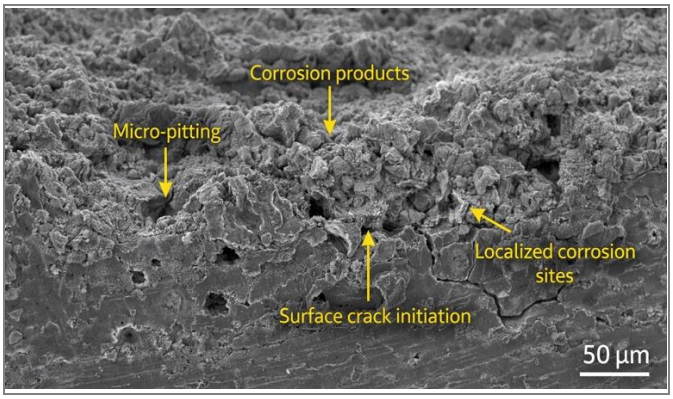

Figure 7. SEM image showing the surface corrosion morphology of welded ST37 low-carbon steel after immersion in NaOH solution, with magnification: 1000x, accelerating voltage: 15

Figure 6 and Figure 7 present SEM observations of welded ST37 low-carbon steel after immersion in NaOH solution, highlighting the evolution of corrosion morphology and surface degradation with increasing exposure time. In Figure 6, the cross-sectional SEM images reveal the distinct microstructural regions of the welded joint, including the fusion zone (FZ),

heat-affected zone (HAZ), and base metal (BM). The uppermost region corresponds to the corrosion product layer formed on the steel surface due to electrochemical interactions between the metal substrate and the basic solution. After 100 hours of immersion (**Figure 6a**), a relatively thin corrosion layer begins to develop on the weld surface. As the exposure time increases to 200 hours (**Figure 6b**) and 300 hours (**Figure 6c**), the corrosion layer becomes progressively thicker and more irregular, indicating the continuous accumulation of corrosion products. The fusion zone shows the most significant degradation due to its heterogeneous microstructure and residual stresses introduced during the welding process, while the HAZ exhibits moderate structural changes. In contrast, the base metal retains a comparatively smoother morphology, indicating lower susceptibility to corrosion.

Figure 7 provides a detailed surface SEM image of the corroded welded steel, illustrating several characteristic corrosion features. The surface morphology shows the formation of porous corrosion products accompanied by localized degradation phenomena such as micro-pitting, localized corrosion sites, and the initiation of surface cracks. These features indicate that corrosion in the NaOH environment occurs through localized dissolution processes followed by the accumulation of corrosion products on the surface. The presence of micro-pits suggests the initiation of localized electrochemical reactions, which gradually propagate and contribute to the development of surface cracks and porous corrosion layers. Overall, the SEM observations demonstrate that prolonged immersion in the basic environment accelerates the formation of corrosion products and promotes localized corrosion mechanisms, particularly in the weld metal region, which ultimately affects the structural integrity of the welded ST37 low-carbon steel. These passive layers act as protective barriers that hinder further corrosion, in agreement with established mechanisms described by Aljibori *et al*. [28], who reported that basic media stabilize the oxide layer on low-carbon steels.

Figure 8 and **Figure 9** present SEM observations of welded ST37 low-carbon steel after immersion in an NH_4Cl solution, illustrating the development of corrosion morphology and surface degradation with increasing exposure time. In **Figure 8**, the cross-sectional SEM micrographs reveal the different microstructural regions of the welded joint, including the fusion zone (FZ), heat-affected zone (HAZ), and base metal (BM). The uppermost region corresponds to the corrosion layer formed on the exposed weld surface due to electrochemical reactions between the steel substrate and the chloride-containing environment. After 100 hours of immersion (**Figure 8a**), a relatively thin corrosion layer begins to form on the weld surface. As the immersion time increases to 200 hours (**Figure 8b**) and 300 hours (**Figure 8c**), the corrosion layer becomes progressively thicker and more irregular, indicating continuous corrosion activity and the accumulation of corrosion products. The fusion zone exhibits more pronounced degradation due to its heterogeneous microstructure and the presence of residual stress generated during the welding process. In comparison, the heat-affected zone shows moderate structural changes, while the base metal retains a relatively smoother morphology with less severe corrosion damage.

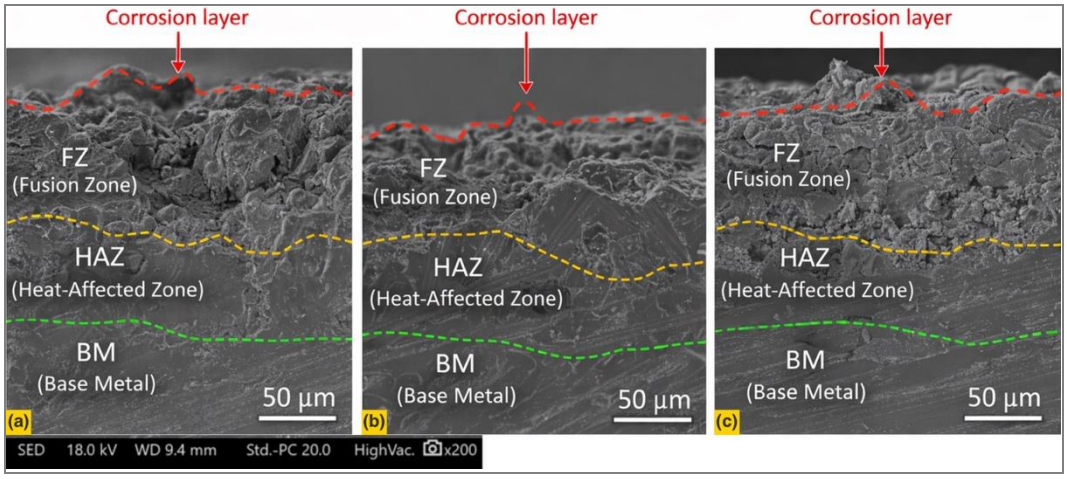

Figure 8. Cross section material ST37 low-carbon steel after immersion NH_4Cl: (a) 100; (b) 200; (c) 300 hours.

Figure 9 provides a higher-magnification SEM image of the corroded surface morphology of welded ST37 steel after exposure to the NH_4Cl solution. The surface is characterized by the presence of corrosion products distributed across the weld surface, accompanied by localized corrosion features such as micro-pitting, coalesced pits, and the initiation of surface cracks. These morphological features indicate that corrosion in the NH_4Cl environment occurs predominantly

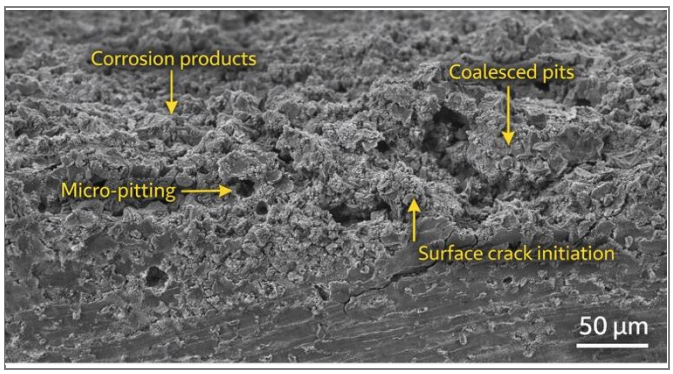

Figure 9. SEM image showing the surface corrosion morphology of welded ST37 low-carbon steel after immersion in NH4Cl solution, with magnification: 1000x, accelerating voltage: 15

through localized electrochemical reactions promoted by chloride ions, which are known to accelerate metal dissolution and destabilize protective oxide films. The formation and growth of micro-pits can lead to pit coalescence and crack initiation, contributing to the development of a rough and porous corrosion layer. Overall, the SEM observations demonstrate that prolonged exposure to the chloride-containing solution intensifies localized corrosion processes, particularly in the weld metal region, which may significantly reduce the durability and structural integrity of welded ST37 low-carbon steel.

3.2. Elemental Composition Analysis

The EDS spectrum of the corroded ST37 low-carbon steel surface after immersion in NaOH solution (**Figure 10**) reveals the dominant presence of iron peaks (FeL, FeK series), confirming the substrate as the primary constituent. The detection of oxygen (OKα) indicates the formation of oxide or hydroxide layers, which are typical corrosion products in basic environments. A minor carbon signal (C Kα) is also observed, likely originating from adsorbed species or surface contamination; however, due to the inherent limitations of EDS in quantifying light elements, these values should be interpreted with caution. Additional peaks corresponding to sodium (NaKα) and aluminum (AlKα) suggest incorporation of electrolyte residues or possible contamination during immersion. The platinum peaks (PtM, PtL series) are attributed to the sputter-coating process applied to improve surface conductivity prior to analysis.

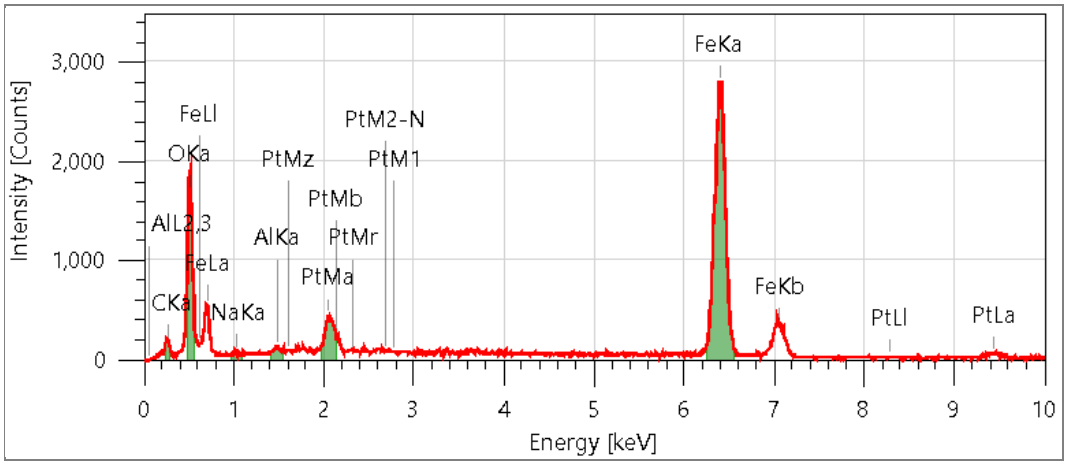

Figure 10. EDS spectrum showing the elemental composition of the corroded surface of ST37 low-carbon steel after immersion in NaOH solution

These findings support the proposed corrosion mechanism, where the basic medium promotes the formation of iron oxides/hydroxides on the steel surface. The strong Fe and O signals confirm the protective but porous nature of the corrosion layer, while the presence of Na indicates interaction with the electrolyte. The semi-quantitative detection of C and O highlights the methodological limitation of EDS for light elements, reinforcing the need to focus on the major alloying constituents when interpreting the corrosion behavior.

The EDS spectrum of the corroded ST37 low-carbon steel surface after immersion in NH_4Cl solution (**Figure 11**) highlights the dominant iron peaks (FeL, FeK series), confirming the steel substrate as the primary constituent. The presence of oxygen (OKα) indicates the formation of iron oxides or hydroxides, which are typical corrosion products in chloride-containing environments. Chlorine peaks (ClKα, ClKβ) are clearly observed, signifying the aggressive role of chloride ions in penetrating the steel surface and accelerating localized corrosion. Nitrogen (N Kα) and carbon (C Kα) signals are also detected, likely originating from the NH_4Cl electrolyte and adsorbed species. Platinum peaks (PtM, PtL series) are attributed to the sputter-coating process applied to improve conductivity during analysis.

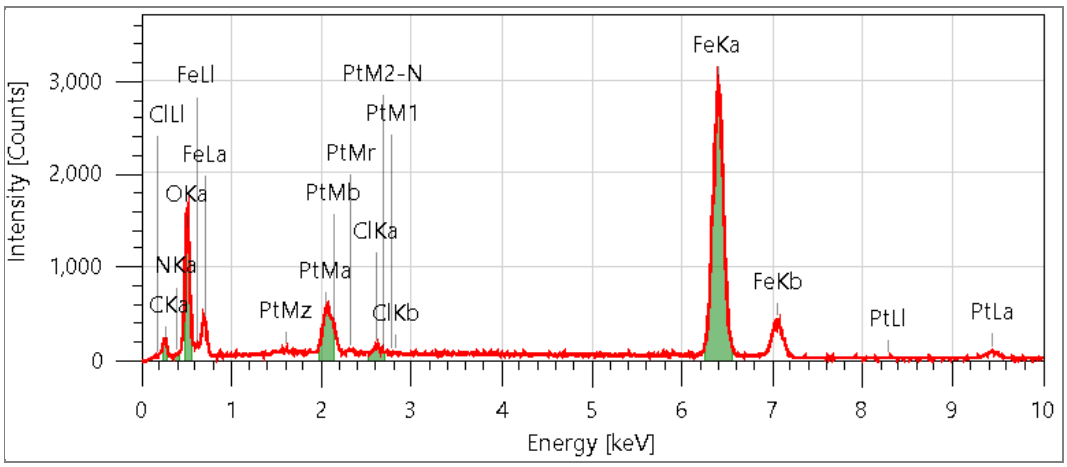

Figure 11. EDS spectrum showing the elemental composition of the corroded surface of ST37 low-carbon steel after immersion in NH_4Cl solution

Overall, the spectrum confirms that immersion in NH_4Cl promotes severe corrosion through chloride ion attack, leading to the formation of iron oxide/hydroxide layers. The simultaneous detection of Cl and O supports the mechanism of localized pitting corrosion, while the nitrogen signal reflects the electrolyte's contribution. These findings reinforce the conclusion that chloride environments are particularly aggressive toward low-carbon steels, producing unstable corrosion layers that compromise surface integrity. The combination of high oxygen and detectable chloride content provides strong evidence of chloride-induced corrosion, as commonly reported in mild steel studies [29], [30].

3.3. Mechanical Properties after Corrosion Exposure

The corrosion rate results presented in **Table 1** clearly demonstrate the different effects of NaOH and NH_4Cl solutions on the corrosion behavior of ST37 low-carbon steel. In the NaOH solution, the corrosion rate values were relatively low, ranging from 0.024 to 0.019 mm/year during the 100–300 hours immersion period. This indicates that the basic environment provided by NaOH promotes the formation of a stable and adherent iron oxide layer on the steel surface. Such passive film formation limits further metal dissolution and acts as a protective barrier against corrosion. The gradual decrease in corrosion rate further supports the idea that the oxide film thickens and stabilizes as immersion continues [2].

The corrosion rate of ST37 low-carbon steel in the NH_4Cl solution was markedly elevated in **Table 2**, commencing at 0.314 mm/year after 100 hours and declining to 0.197 mm/year after 300 hours. The elevated initial corrosion rate is ascribed to the aggressive characteristics of chloride ions, which compromise the passive oxide layer and facilitate localized corrosion, including pitting [31], [32]. The observed decrease in corrosion rate with increasing immersion time is likely attributed to the formation and accumulation of corrosion products on the material surface. These corrosion layers act as a temporary protective barrier, partially blocking active sites and reducing further corrosive attack.

Overall, the findings suggest that NaOH solution provides a protective environment, while NH_4Cl solution induces more aggressive corrosion, consistent with the general understanding that chloride-containing environments are highly detrimental to steel materials.

Table 1. Calculation of corrosion rate for specimens after immersion in NaOH solution

Immersion time (hours)	Weight Loss ΔW (g)	Constant (C)	Density P (g/cm³)	Surface Area ΔA (cm²)	Corrosion Rate (mmpy)
100	0.004	87.600	7.86	19.767	0.024
200	0.006	87.600	7.86	19.763	0.017
300	0.010	87.600	7.86	19.756	0.019

Table 2. Calculation of corrosion rate for specimens after immersion in NH_4Cl solution

Immersion time (hours)	Weight Loss ΔW (g)	Constant (C)	Density P (g/cm³)	Surface Area ΔA (cm²)	Corrosion Rate (mmpy)
100	0.055	87.600	7.86	19.649	0.314
200	0.081	87.600	7.86	19.602	0.230
300	0.104	87.600	7.86	19.568	0.197

The tensile test findings for ST37 low-carbon steel el18ucidate the alterations in the material's mechanical properties following immersion in a corrosive solution for varied durations (**Table 3**). For specimens immersed in NaOH solution, the yield strength and tensile strength exhibited a

noticeable variation with immersion duration. The yield strength decreased significantly at 200 hours (176.81 N/mm²), indicating surface degradation and possible microstructural weakening due to the basic environment. However, a partial recovery in strength at 300 hours (266.11 N/mm²) suggests the formation of a passive oxide layer that temporarily inhibited further corrosion.

In contrast, the NH4Cl immersed specimens consistently showed higher yield and tensile strength values compared to those immersed in NaOH. The highest tensile strength of 406.46 N/mm² was recorded after 100 hours, followed by a slight reduction at 200 and 300 hours. The presence of chloride ions (Cl^-) in the NH_4Cl solution promoted localized pitting and surface roughness, which initially increased dislocation density and apparent strength but eventually led to mechanical deterioration. The initial high strength could result from surface hardening effects due to chloride-induced pitting, but prolonged exposure likely caused deep localized damage and microcrack formation, reducing the material's load-bearing capacity.

Table 3. Tensile test for specimen ST37 low-carbon steel

No	Specimen with Immersion	Max. Force (N)	Yield Strength (N/mm²)	Tensile Strength (N/mm²)
1	NaOH 100 hours	49.520	257,06	356,49
2	NaOH 200 hours	43.487	176,81	202,95
3	NaOH 300 hours	46.527	266,11	368,56
4	NH_4Cl 100 hours	51.333	313,46	406,46
5	NH_4Cl 200 hours	50.249	306,81	394,77
6	NH_4Cl 300 hours	42.809	324,63	357,93

The initial reduction in mechanical strength indicates that exposure to the NaOH solution promotes active corrosion and surface degradation of the welded ST37 steel. The formation of corrosion products and the development of microcracks reduce the effective load-bearing capacity of the material, as reflected in the decrease of yield strength and tensile strength values (**Figure 12**). After 200 hours of immersion, the material exhibited the lowest yield strength (176.81 N/mm²) and tensile strength (202.95 N/mm²), suggesting that prolonged basic exposure can induce localized corrosion and microstructural weakening of the steel matrix. However, a slight increase in strength observed after 300 hours may be associated with the development of a relatively more stable corrosion layer on the surface. The presence of this layer can partially limit the direct interaction between the electrolyte and the underlying metal, thereby temporarily reducing corrosion penetration and contributing to a modest recovery in the measured mechanical properties.

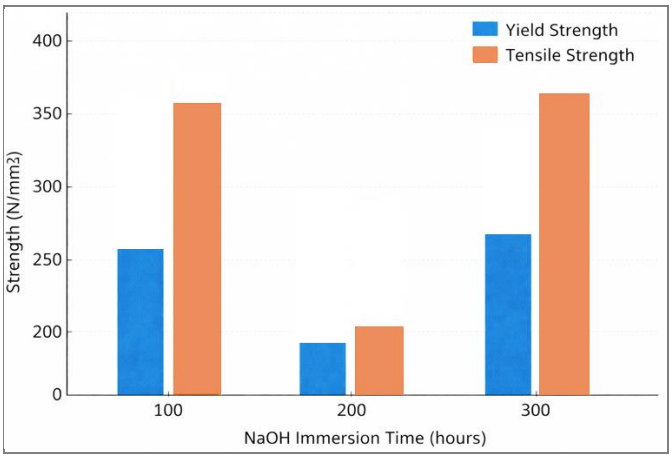

Figure 12. Tensile test with variable immersion time for NaOH solution

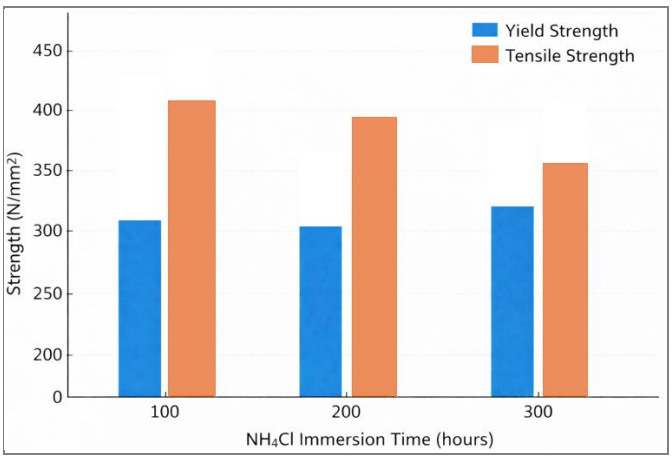

Figure 13. Tensile test with variable immersion time for NH_4Cl solution

Figure 13 illustrates the changes in yield strength and tensile strength of ST37 low-carbon steel following immersion in an NH_4Cl solution for several durations. After 100 hours, the yield strength is 313.46 N/mm² and the tensile strength is 406.46 N/mm². With an immersion duration extending to 200 hours, both metrics exhibit a modest reduction to 306.81 N/mm² and 394.77 N/mm², indicating a minor decline in load-bearing ability attributed to the onset of localized corrosion and pitting. After 300 hours, the tensile strength decreases to 357.93 N/mm², however the yield strength marginally increases to 324.63 N/mm², indicating partial stability of the corrosion layer. Chloride ions expedite electrochemical reactions by infiltrating and degrading passive

oxide coatings, resulting in pitting and intergranular corrosion on the steel surface. Prolonged exposure to the corrosive environment may lead to the accumulation of corrosion products on the steel surface. The presence of these products may form a surface layer that partially covers the substrate, which can influence the corrosion behavior by reducing the direct interaction between the electrolyte and the metal surface. In contrast to NaOH immersion, NH_4Cl exposure leads to a more uniform but comparatively slower degradation, indicating a less aggressive attack on the steel microstructure. The results suggest that the chloride environment primarily reduces mechanical strength by damaging the surface layer and initiating localized pitting corrosion, which progressively develops with increasing immersion time.

This study's results directly fulfill the primary research objectives, which sought to assess the impact of basic (NaOH) and acidic (NH_4Cl) conditions on the corrosion behavior and mechanical deterioration of ST37 low-carbon steel. The results indicate that exposure to NaOH leads to an initial decline in mechanical strength, succeeded by a partial restoration, which aligns with the development of a protective passive oxide layer that restricts additional corrosion. Conversely, exposure to NH_4Cl resulted in ongoing material degradation due to chloride ion infiltration, which facilitates localized pitting and undermines passive film integrity. The results validate the premise presented in the introduction that chloride-containing conditions are considerably more corrosive to steel than basic environments. Moreover, the SEM and EDX tests corroborate these findings by indicating greater surface degradation and elevated chloride concentration in NH_4Cl specimens. The study effectively achieves its objectives by clarifying the unique corrosion mechanisms in various environments and quantifying their impact on tensile properties, offering significant insights into the long-term performance of mild steel under industrial or environmental conditions with basic or acidic exposure.

The variation in corrosion behavior with increasing immersion time in the NaOH solution can be correlated with the evolution of surface morphology observed in the SEM images. After 100 hours of immersion, the steel surface exhibited localized corrosion features and the initial formation of corrosion products, indicating the early stage of surface degradation. At 200 hours, the SEM micrographs revealed a relatively more compact and continuous corrosion layer partially covering the surface. The formation of this layer may temporarily limit the direct contact between the electrolyte and the underlying metal, resulting in a reduction in the corrosion response. However, with prolonged immersion up to 300 hours, the corrosion layer appeared increasingly porous and locally damaged, as indicated by the presence of cracks, pits, and a rougher surface morphology. The breakdown or instability of this surface layer likely facilitates renewed electrolyte penetration and accelerates further corrosion propagation at longer exposure times.

4. Conclusion

This study evaluated the corrosion behavior and mechanical degradation of welded ST37 low-carbon steel in basic (NaOH) and chloride-containing (NH_4Cl) environments using gravimetric measurements, SEM–EDS characterization, and tensile testing. The results indicate that environmental chemistry and immersion time significantly influence corrosion mechanisms and structural performance. Exposure to NaOH promoted the formation of a relatively stable oxide layer that reduced corrosion kinetics and resulted in lower corrosion rates (0.024–0.019 mm/year), while SEM observations confirmed the presence of a more compact corrosion layer with limited surface damage. In contrast, NH_4Cl exposure produced more aggressive corrosion characterized by pitting, porous corrosion products, and localized surface deterioration associated with chloride-induced passive film breakdown. EDS analysis supported these observations through the detection of oxygen-rich oxide layers in NaOH environments and chloride species in NH_4Cl-exposed samples. Mechanical testing further showed that NaOH exposure caused temporary mechanical degradation followed by partial recovery due to passivation effects, whereas NH_4Cl immersion led to continuous tensile strength reduction associated with pit formation and microstructural damage. These findings highlight the critical role of environmental chemistry in controlling corrosion behavior and mechanical integrity of welded low-carbon steel in industrial applications.

Acknowledgements

The authors would like to express their sincere gratitude to the Directorate of Research, Technology, and Community Service (DPPM Kemdiktisaintek) Research Grant Number 0419/C3/DT.05.00/2025; 126/C3/DT.05.00/PL/2025; and 6/KP-DRP-RISET/VI/2025 for providing

financial support through the research grant. Appreciation is also extended to the Research and Innovation Center (RIC) of Universitas Muhammadiyah Yogyakarta (UMY) for its valuable guidance and continuous support throughout the research process.

Authors' Declaration

Authors' contributions and responsibilities – Conceptualization, A.W. and M.; Methodology, A.W.; S.M.; Validation, A.W. and M.; Formal analysis, A.W.; S.M. and S.; Investigation, A.W.; S.M. and S.; Resources, A.W. and M.; Data curation, A.W. and M.; Writing—original draft preparation, A.W. and H.B.; Writing—review and editing, A.W. and H.B. All authors have read and agreed to the published version of the manuscript.

Funding – Directorate of Research, Technology, and Community Service (DPPM Kemdiktisaintek) Research Grant Number 0419/C3/DT.05.00/2025; 126/C3/DT.05.00/PL/2025; and 6/KP-DRP-RISET/VI/2025.

Availability of data and materials – All data is available from the authors.

Competing interests – The authors declare no competing interests.

Additional information – No additional information from the authors.

References

[1] K. C. Manu, C. Madhushree, M. S. Chandini, N. Shree, S. Hemanth, and T. P. Jeevan, "Corrosion in Steel Structures: A Review," *Journal of Mines, Metals and Fuels*, vol. 73, no. 1, pp. 189–198, Jan. 2025, doi: 10.18311/jmmf/2025/46985.

[2] R. Bender *et al.*, "Corrosion challenges towards a sustainable society," *Materials and Corrosion*, vol. 73, no. 11, pp. 1730–1751, Nov. 2022, doi: 10.1002/maco.202213140.

[3] S. H. Khazaal and H. F. Makki, "Characterization of Corrosion Behavior of ST37-2 Low-Carbon Steel in a Cooling Tower Using Seawater as the Working Media," *Journal of Bio- and Tribo-Corrosion*, vol. 11, no. 4, p. 97, Dec. 2025, doi: 10.1007/s40735-025-01018-4.

[4] G. P. V. Dalmora, E. P. Borges Filho, A. A. Maraschin Conterato, W. S. Roso, C. E. Pereira, and A. Dettmer, "Methods of corrosion prevention for steel in marine environments: A review," *Results in Surfaces and Interfaces*, vol. 18, p. 100430, Jan. 2025, doi: 10.1016/j.rsurfi.2025.100430.

[5] S. A. Galedari, A. Mahdavi, F. Azarmi, Y. Huang, and A. McDonald, "A Comprehensive Review of Corrosion Resistance of Thermally-Sprayed and Thermally-Diffused Protective Coatings on Steel Structures," *Journal of Thermal Spray Technology*, vol. 28, no. 4, pp. 645–677, Apr. 2019, doi: 10.1007/s11666-019-00855-3.

[6] A. Vafadar, F. Guzzomi, A. Rassau, and K. Hayward, "Advances in Metal Additive Manufacturing: A Review of Common Processes, Industrial Applications, and Current Challenges," *Applied Sciences*, vol. 11, no. 3, p. 1213, Jan. 2021, doi: 10.3390/app11031213.

[7] T. Lehmann *et al.*, "Large-scale metal additive manufacturing: a holistic review of the state of the art and challenges," *International Materials Reviews*, vol. 67, no. 4, pp. 410–459, May 2022, doi: 10.1080/09506608.2021.1971427.

[8] R. A. Himarosa *et al.*, "Simultaneous Double-Sided Metal Inert Gas Welding of AA5052 Aluminum Alloy T-Joints," *Materials Science Forum*, vol. 1067, pp. 53–59, Aug. 2022, doi: 10.4028/p-t0072n.

[9] H.-C. Chen, A. Wisnujati, Mudjijana, A. M. Widodo, and C.-W. Lung, "Grey Relational Analysis and Grey Prediction Model (1, 6) Approach for Analyzing the Electrode Distance and Mechanical Properties of Tandem MIG Welding Distortion," *Materials*, vol. 16, no. 4, p. 1390, Feb. 2023, doi: 10.3390/ma16041390.

[10] M.-T. Chen, Y. Pan, F. Ren, H. Cao, M. Lai, and J. Zhang, "Experimental investigation and predictive model on tensile behavior of corroded high-strength steel and butt-welded connections," *Thin-Walled Structures*, vol. 210, p. 112982, May 2025, doi: 10.1016/j.tws.2025.112982.

[11] M. Rajbanul Akhond, A. Irfan, and A. Sharif, "An overview of corrosion behavior and contemporary management techniques of thermomechanically treated rebars in concrete

structures," *Journal of Structural Integrity and Maintenance*, vol. 9, no. 1, p. 2259721, Jan. 2024, doi: 10.1080/24705314.2023.2259721.

[12] R. T. Loto, S. Oladipupo, T. Folarin, and E. Okosun, "Impact of chloride concentrations on the electrochemical performance and corrosion resistance of austenitic and ferritic stainless steels in acidic chloride media," *Discover Applied Sciences*, vol. 7, no. 7, p. 672, Jun. 2025, doi: 10.1007/s42452-025-07234-4.

[13] Y. Huang *et al.*, "Microstructure and corrosion characterization of weld metal in stainless steel and low carbon steel joint under different heat input," *Materials Today Communications*, vol. 29, p. 102948, Dec. 2021, doi: 10.1016/j.mtcomm.2021.102948.

[14] S. Antony Jose *et al.*, "Wear- and Corrosion-Resistant Coatings for Extreme Environments: Advances, Challenges, and Future Perspectives," *Coatings*, vol. 15, no. 8, p. 878, Jul. 2025, doi: 10.3390/coatings15080878.

[15] J. L. Bañuelos *et al.*, "Oxide– and Silicate–Water Interfaces and Their Roles in Technology and the Environment," *Chemical Reviews*, vol. 123, no. 10, pp. 6413–6544, May 2023, doi: 10.1021/acs.chemrev.2c00130.

[16] S. T. Fasasi, O. J. Adebowale, and Z. Q. S. Nwokediegwu, "Sensor Technology Performance under Environmental Interference: A Comparative Evaluation Model," *International Journal of Scientific Research in Computer Science, Engineering and Information Technology*, vol. 10, no. 3, pp. 843–855, 2024, doi: https://ijsrcseit.com/index.php/home/article/view/CSEIT25113468.

[17] K. Li *et al.*, "Influence of Partial Rust Layer on the Passivation and Chloride-Induced Corrosion of Q235b Steel in the Carbonated Simulated Concrete Pore Solution," *Metals*, vol. 12, no. 7, p. 1064, Jun. 2022, doi: 10.3390/met12071064.

[18] S. Palanivelu, S. Avudaiappan, and N. Maureira-Carsalade, "Corrosion behaviour of mild steel in diverse environments: a comparative study of hot-rolled and cold-rolled specimens," *Journal of King Saud University – Engineering Sciences*, vol. 37, no. 6, p. 29, Oct. 2025, doi: 10.1007/s44444-025-00038-2.

[19] D. Tyrała and B. Pawłowski, "Microstructural Aspects of Premature Pitting Corrosion of Steel Pipe–Case Study," *Journal of Failure Analysis and Prevention*, vol. 22, no. 6, pp. 2147–2153, Dec. 2022, doi: 10.1007/s11668-022-01530-6.

[20] M. Dada and P. Popoola, "Recent advances in joining technologies of aluminum alloys: a review," *Discover Materials*, vol. 4, no. 1, p. 86, Dec. 2024, doi: 10.1007/s43939-024-00155-w.

[21] M. Fedel, J. Franch, and S. Rossi, "Effect of thickness and sealing treatments on the corrosion protection properties of anodic oxide coatings on AA5005," *Surface and Coatings Technology*, vol. 408, p. 126761, Feb. 2021, doi: 10.1016/j.surfcoat.2020.126761.

[22] M. Mudjijana, R. A. Himarosa, and S. Sudarisman, "Macro-Micro Analysis on 2-Layer Semiautomatic MIG Welding of AA5052 Material Using ER5356 Electrode," *Key Engineering Materials*, vol. 867, pp. 204–212, Oct. 2020, doi: 10.4028/www.scientific.net/KEM.867.204.

[23] M. Mohammadi Soleymani, E. Mehrabi Gohari, and A. Zahedian, "Evaluation of Mechanical Properties of Welding ST-37 Steel Structures With Two Types of Welding Processes FCAW and SMAW," *International Journal of Iron & Steel Society of Iran*, vol. 21, no. 1, pp. 33–44, 2024, doi: 10.22034/ijissi.2024.2035314.1297.

[24] Z. Zhang, H. Wang, H. Qian, Q. Feng, X. Jin, and F. Fan, "Comparative analysis and applicability of corrosion test methods for construction steel components," *Case Studies in Construction Materials*, vol. 18, p. e02034, Jul. 2023, doi: 10.1016/j.cscm.2023.e02034.

[25] W. Liu *et al.*, "Corrosion resistance and corrosion interface characteristics of Cr-alloyed rebar based on accelerated corrosion testing with impressed current," *Journal of Materials Research and Technology*, vol. 22, pp. 2996–3009, Jan. 2023, doi: 10.1016/j.jmrt.2022.12.136.

[26] N. Kato, M. Yamada, J. Ojima, and M. Takaya, "Analytical method using SEM-EDS for metal elements present in particulate matter generated from stainless steel flux-cored arc welding process," *Journal of Hazardous Materials*, vol. 424, p. 127412, Feb. 2022, doi: 10.1016/j.jhazmat.2021.127412.

[27] F. Soleymani, "Internal Corrosion Monitoring of Pipelines Using Electrochemical Techniques: A Comprehensive Review," *Protection of Metals and Physical Chemistry of Surfaces*, vol. 59,

no. 5, pp. 1045–1061, Nov. 2023, doi: 10.1134/S207020512370096X.

[28] H. Aljibori, A. Alamiery, and A. Kadhum, "Advances in corrosion protection coatings: A comprehensive review," *Internation Journal Corrosion Scale Inhibitor*, vol. 12, no. 4, pp. 1476–1520, 2023.

[29] W. Feng, A. Tarakbay, S. Ali Memon, W. Tang, and H. Cui, "Methods of accelerating chloride-induced corrosion in steel-reinforced concrete: A comparative review," *Construction and Building Materials*, vol. 289, p. 123165, Jun. 2021, doi: 10.1016/j.conbuildmat.2021.123165.

[30] P. Bajić, B. Leporace-Guimil, C. Andrade, N. Tošić, and A. de la Fuente, "Chloride-Induced Corrosion Effects on the Structural Performance of Concrete with Rebar and Fibres: A Review," *Applied Sciences*, vol. 15, no. 12, p. 6457, Jun. 2025, doi: 10.3390/app15126457.

[31] H. Parangusan, J. Bhadra, and N. Al-Thani, "A review of passivity breakdown on metal surfaces: influence of chloride- and sulfide-ion concentrations, temperature, and pH," *Emergent Materials*, vol. 4, no. 5, pp. 1187–1203, Oct. 2021, doi: 10.1007/s42247-021-00194-6.

[32] D. B. Wang, S. D. Zhang, Q. Wang, L. M. Zhang, and J. Q. Wang, "Underlying mechanism for the effects of composition and microstructure on the corrosion resistance of Al-based amorphous alloys: a review," *Critical Reviews in Solid State and Materials Sciences*, vol. 49, no. 6, pp. 1120–1152, Nov. 2024, doi: 10.1080/10408436.2024.2311414.